

Brain Cortical Stimulation Thresholds to Different Magnetic Field Sources Exposures at Intermediate Frequencies

Jose Gomez-Tames, *Member, IEEE*, Thomas Tarnaud, Keishi Miwa, Akimasa Hirata, *Fellow, IEEE*, Tom Van de Steene, Luc Martens, *Member, IEEE*, Emmeric Tanghe, Wout Joseph, *Senior Member, IEEE*

Abstract— Permissible field strengths in the international guidelines/standard for human protection are derived from peripheral nerve system stimulation at the intermediate frequencies where electrostimulation (attributable to axon activation) is more dominant than thermal effect. Recently, multi-scale computation is used to investigate neuron stimulation thresholds by incorporating individual neurons into realistic head models. However, the consistency of excitation models and permissible levels to specific target tissues (central nervous system) needs to be clarified. This study aims to investigate brain cortical stimulation thresholds using a multi-scale computational approach for different scenarios of magnetic field exposures. The magnetic exposures include transcranial magnetic stimulation, uniform exposure, and wireless power transfer systems. Our results confirmed the consistency of the multi-scale computations of the cortical thresholds between two independent groups for electromagnetic exposure of transcranial magnetic stimulation (thresholds in the range of motor cortex activation). We also quantified the conservativeness of permissible field strengths of international guidelines/standards at intermediate frequencies. Finally, with the multi-scale approach, we confirmed that ten thousand kW of transmitting power of wireless power transfer (WPT) in an electric vehicle charging system may not induce an adverse effect for cortical activation.

Index Terms— Dosimetry, Human safety, Nerve model, Multi-scale, Standardization, Transcranial magnetic stimulation (TMS), Wireless power transfer (WPT)

I. INTRODUCTION

THERE have been concerns about potential adverse health effects of human exposure to electromagnetic fields. The dominant effect for instantaneous exposure is the electrostimulation at frequencies lower than 5 MHz [1] and 10 MHz [2], while a thermal effect for constant exposure (> 6-min average) is described at the frequencies higher than 100 kHz in the international exposure standards/guidelines [1], [2]. In the standards/guidelines, a safety/reduction factor is applied to

known or operational thresholds to derive permissible internal physical quantities. However, the threshold assessment for the pain or sensory effect is limited in the intermediate-frequencies (IF) range where the stimulation is attributable to axon activation. The IF range is defined between 300 Hz to 10 MHz, according to WHO [3] or 300 Hz to 1 MHz in [4]. In this study, the definition of WHO is followed.

In the IEEE C95.6 standards, the nerve activation model named SENN is used to relate the electric field and nerve activation, and then the ellipsoid, mimicking the human body parts, is used to relate the external magnetic field and internal electric field. In the ICNIRP 2010 guidelines [5], the activation model has not been mentioned clearly, while anatomical model computation is used to relate the external magnetic field and internal electric field. To derive a threshold in a scientific manner, the combination of the electromagnetic dosimetry and neuron model (multi-scale computation) is listed in the research agenda of the IEEE International Committee on Electromagnetic Safety (ICES) [6]. A working group on ‘Exploring the electrostimulation threshold in the brain’ has been established in the IEEE ICES Technical Committee 95 Subcommittee 6 to clarify certain aspects and is led by the authors. The mission of the working group includes the assessment of the cortical stimulation threshold variability by combining electromagnetic dosimetry and central nervous system (CNS) neuron models. In the guidelines/standard, the threshold of PNS pain and CNS stimulation (sensory effect), which are not straightforward to compare, has not been evaluated at the intermediate frequencies.

In addition, new frequency bands will be used in wireless power transfer (WPT) systems [7], [8]. Promising frequency bands are spread, from kHz to lower MHz range, which coincides with the above-mentioned frequency range for electrostimulation effects. Even though the transmission efficiency in WPT systems is high enough, leaked field strength

Manuscript submitted May 31, 2019. This work was supported in part by JSPS KAKENHI 17H00869 under Grant-in-Aid for Young Scientist (J. GT) and by the Ghent University Special Research Fund project “Assessment of human exposure to intermediate-frequency electromagnetic fields originating from wireless power transfer systems”.

J. Gomez-Tames (correspondence e-mail: jgomez@nitech.ac.jp), T. Miwa (k.miwa.454@stn.nitech.ac.jp), A. Hirata (ahirata@nitech.ac.jp) are with the

Department of Electrical and Mechanical Engineering, Nagoya Institute of Technology, 466-8555 Nagoya, Japan.

T. Tarnaud (Thomas.Tarnaud@UGent.be), T. Van de Steene (Tom.VandeSteene@UGent.be), L. Martens (Luc1.Martens@UGent.be), E. Tanghe (Emmeric.Tanghe@UGent.be), W. Joseph (Wout.Joseph@UGent.be) are with the Department of Information Technology Ghent University/IMEC, Ghent, Belgium. T. Tarnaud is a PhD Fellow of the FWO-V (SB) (Research Foundation Flanders, Belgium).

may not be ignored because of its high transmission power. The compliance assessment for WPT has been conducted by different groups [8]–[14], including electric vehicle charge [15]–[20]. In addition, the leaked magnetic field from induction heating (IH) cooking hobs would also be similar [4], [21]–[23]. The waveform/signal in such systems is close to continuous sinusoidal waves, in which the heating should be applied for the latter. However, both considerations are needed in kHz band.

Computational dosimetry becomes an essential tool for estimating induced physical quantities [24]. There is an increasing trend in incorporating individual neurons into realistic head models that can be used to investigate neuron stimulation thresholds for medical applications [25]–[33] and recently for dosimetry studies [28]. However, the consistency of excitation models for a specific target tissue needs to be investigated. This issue is also listed in the research agenda of the IEEE ICES [6]. Moreover, due to ethical problems, it is difficult to evaluate the threshold of electrostimulation in humans for non-medical applications. One common non-invasive brain stimulation technique is transcranial magnetic stimulation (TMS) [34], [35], in which stimulation thresholds can be determined by measuring the motor-evoked potential. The current flowing in the coil of TMS induces an eddy current in the human tissue to activate a target area. A common marker to TMS physiological responses is the motor evoked potential (MEP). The most common protocol is to adjust the position of the TMS coil to target a muscle of the hand with the lowest intensity to obtain the motor threshold values of the MEP. The threshold for MEPs is used in the clinical application as a percentage of the maximum stimulation output of the stimulation device. However, the internal electric field for stimulation threshold in the brain is unknown from in-vivo human measurements.

In this study, the aim is to estimate the activation of cortical axons by the induced internal electric field to derive and discuss conservativeness of permissible field strengths in the international guidelines/standards (i.e., reference levels) for IF frequencies defined between 1 kHz to 10 MHz. The internal electric field computation and nerve modelling methods have been conducted and verified by two independent groups for TMS exposure. This multi-scale approach was applied to derive permissible field strengths of standards/guidelines and to evaluate potential stimulation for exposure from the WPT system for electric vehicle charge. Preliminary results of this work were presented in [36].

II. MODELS AND METHODS

A. Human Head Model

A freely available magnetic resonance image (MRI) database is used to create a realistic head model (available on <http://hdl.handle.net/1926/1687>). The head model consisted of 14 tissues/body fluids [37], [38]. The model was voxelized with a resolution of 0.5 mm (65.3×10^6 voxels).

B. Electromagnetic Computational Method

At the intermediate frequencies, the electric and external

magnetic fields are decoupled, and it is possible to treat the exposure to these fields separately. In most practical exposure scenarios at the intermediate frequencies, the magnetic field is dominant compared to the electric field. Also, the conduction currents are at least one order of magnitude higher than the displacement currents, and therefore, in most of the scenarios, only tissue conductivity should be considered; the permittivity can be neglected [39], [40]. Thus, the induced scalar potential ϕ is given by the following equation:

$$\nabla \cdot \sigma \nabla \phi = -\nabla \cdot \sigma \frac{\partial \mathbf{A}}{\partial t}, \quad (1)$$

where A and σ denote the magnetic vector potential of the applied (external) magnetic field and tissue conductivity, respectively. The induced electric field is calculated from

$$\mathbf{E} = -\nabla \phi - \frac{\partial}{\partial t} \mathbf{A}. \quad (2)$$

Equation (1) was solved numerically by scalar potential finite difference (SPFD [39]) carried out by Nagoya Institute of Technology, and finite element method (FEM) with rectilinear elements using Sim4Life software carried out by Ghent University [41]. The time evolution of the internal electric field was assumed to be identical to the measured one [42]. Its peak value was computed by SPFD or FEM methods at the operating frequency of the TMS device at each voxel. Finally, the electric field was scaled by a factor of 2.65 to adjust the effect of all present frequency components in the TMS waveform spectrum instead of only one frequency component [27]. In the same way, the scalar potential waveform was obtained. Tissue conductivities were assumed to be linear and isotropic and then determined using the fourth-order Cole-Cole model [43] at the frequencies corresponding to different exposure scenarios. In the case of TMS, the conductivity values were chosen at 10 kHz, as they are experimentally more accurate [44] and close to the operating frequency of the TMS device [42].

In the SPFD solver, the matrix equation was solved iteratively using the geometric multigrid method with successive over-relaxation [45]. By defining scalar potentials (unknowns) at each node of a cubic voxel, a branch current flowing from one node to a neighboring node along the side of the voxels was derived. This branch current included a scalar potential owing to the applied external vector potential and the impedance between nodes. The electric field along the edge of the voxel was obtained by dividing the difference in potential between the nodes of the voxel by the distance across the nodes, then adding the vector potential.

In the Sim4life FEM solver, similarly to the SPFD method, the ohmic-dominated magneto quasistatic equation is used to calculate the electric potential, while the vector potential is evaluated from the Biot-Savart equation. The FEM-equations are solved with the GMRES (generalized minimal residual) method, with absolute and relative convergence tolerance of 1×10^{-50} and 1×10^{-8} , respectively. Raw voxel data was imported in Sim4life from which surfaces are extracted with built-in imaging tools, without post-processing (no smoothing or

simplification) of the obtained surfaces.

C. Neuronal Activation Computational Models

The brain activity generated by external fields is investigated by computing the activation threshold to propagate action potentials using thick pyramidal axons projected from the hand motor cortex (hand knob), as shown in Fig. 1. The activation threshold is given by the internal electric field, or external magnetic field strength required.

The spatially extended nonlinear nodal (SENN [46]) model is used to represent the structure of the axon. The myelinated axon consists of internodes (segments covered by a myelin sheath) concatenated with nodes of Ranvier (ionic channels). The leak conductance of the myelinated internodes was modeled as a passive element or set to zero. The ionic membrane current at the nodes of Ranvier is formulated as a conductance-based voltage-gated model. In this study, the Chiu–Ritchie–Rogart–Stagg–Sweeney (CRRSS) model was used [47]. The SENN axonal representation with CRRSS nodal model was implemented independently by two research groups: Nagoya Institute of Technology (referred here as NITech model [33], [48]) and Ghent University (referred here as SENN-M model) [49]. The NITech and SENN-M models used the same set of parameters in Table A (appendix).

The generated electric potential (extracellular potential V_e), driving the brain activity, is coupled to the membrane potential equation of the axon model at each node and internode $V_m = V_i - V_e$, where V_i is the intracellular membrane potential obtained from the cable equation of the axon model. The elicitation of an action potential was indicated by the depolarization of the transmembrane potential by 50 mV, in at least four consecutive nodes of Ranvier using an in-house code.

For deriving the permissible field strengths in Fig. 4 and Table II, we considered the minimum activation threshold among any of the axons descending from the hand motor area as a strict condition to derive internal electric fields for investigating conservativeness of the guideline/standard. Also, fast-conducting thickly myelinated pyramidal tract axons (Betz cell's axon) were considered for the hand motor area (10 μm in diameter [50]).

D. Exposures Scenarios

For the TMS exposure (Fig. 1A), a 70 mm figure-eight coil was modeled as a single loop of thin. This approximation is appropriate for the coil-to-cortex distance in humans [51], [52]. The TMS coil was placed in two different positions for different exposure studies. One was set over the scalp vertex (Cz position in the 10-20 system) with a medial-lateral orientation of the coil parallel to the longitudinal fissure (subsection III.A). The other was configured to stimulate the putative hand motor area (M1) for dosimetry based on the cortical axon activation (subsection III.B). The optimal coil orientation was along the anterior-posterior orientation and perpendicular to the central sulcus, which is a well-known orientation for stimulating the motor cortex. The stimulation position on the scalp was optimized for the maximum electric field strength in M1, as illustrated in Fig. 1A.

For uniform exposure (Fig. 1B), we considered the IF band (1 kHz, 10 kHz, 100 kHz, 1 MHz, and 10 MHz) to investigate nerve activation to derive reference levels. The list of conductivity value for each tissue at the different frequencies are presented in Table B (appendix). The exposure was for a plane wave in the lateral–medial direction to activate the pyramidal axons by a continuous sinusoidal stimulation (Fig. 1B). We selected the anterior–posterior direction as it generated the smaller thresholds in comparison to the other two conventional uniform plane wave exposure directions (anterior–posterior and superior–inferior). The anterior–posterior direction had an optimal polarization of the fibers in the putative hand motor area.

For the WPT exposure (Fig. 1C), two resonant coils were placed below the center of the vehicle body [53], [54]. The rectangular transmitting coil has a length of 580 mm and a width of 420 mm. The number of turns of the transmitting coil is 15. The square receiving coil has a side of 320 mm. The primary and secondary coils have a separation of 150 mm and misaligned (100 mm in the side-to-side direction and 75 mm in front-to-back direction) based on SAE J2954 [55], as shown in Fig. 1C. The magnetic field leaked from the vehicle, in this case, is larger than that in the case where the coils are exactly aligned, corresponding to the exposure scenario of the worst case. The coils are also modelled as perfectly conducting wires. The transmitting power in normal operation was set to 3.7 kW, and the transfer frequency was 85 kHz [55]. The material of the vehicle is iron with dimensions equivalent to commercial ones. The head is placed in different orientations at 500 mm from the

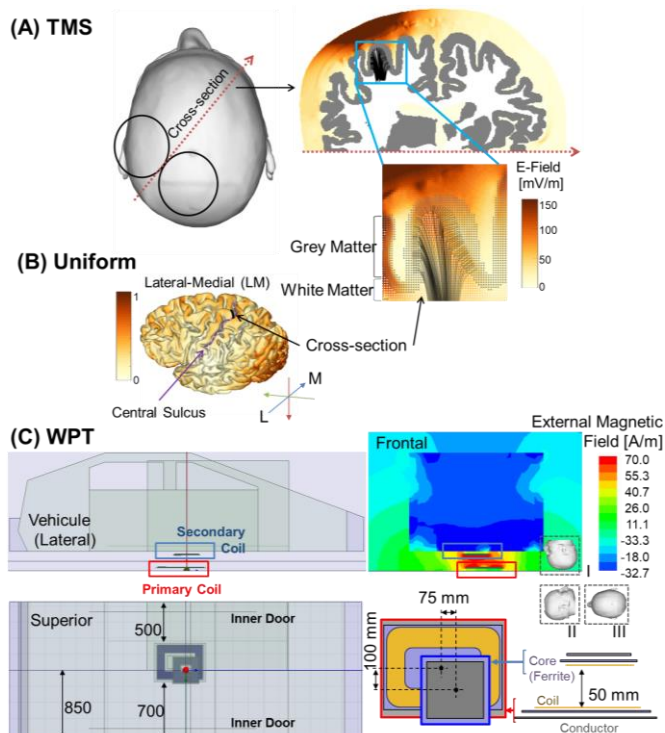


Fig. 1. Exposure scenarios for activation of cortical axons projecting from the hand motor area for three exposures. (A) Illustration of TMS (transcranial magnetic stimulation) exposure over the hand motor area. The pyramidal axons pathways are placed in a cross-section plane. (B) Illustration of uniform exposure and generated internal electric field on the brain surface for lateral-medial direction. (C) Wireless power transfer (WPT) system in an electrical vehicle for dosimetry of head model.

border of the considered WPT system to the nearest scalp surface. Also, the minimum transmitting power was evaluated to achieve the activation of any of the cortical axons.

E. Data Analysis

The maximum internal electric field is used as a metric to derive the reference levels in the standards. Post-processing methods are adopted to systematically suppress outliers in the maximum values that are inherent when using voxelized anatomical models, in which curved boundaries are discretized with a stair-casing approximation. The 99th percentile value of the field strength is considered to remove computational artifacts [5], [56]–[58]. However, for non-uniform exposure, the 99th percentile value is not conservative for compliance purposes. Thus, in addition to 99th percentile value, we used the 99.9th percentile value for practical compromise, which is shown to be consistent with other post- or pre-processing methods to remove the stair-casing error.

Two metrics are used to investigate the difference in the electric field computation using two different electromagnetic solvers (SPFD and FEM). The local difference is the relative percentage difference between the maximum electric values adopting post-processing methods to suppress outliers in the grey matter (99.9th percentile, 99th percentile, and $2 \times 2 \times 2 \text{ mm}^3$ adopting 99.9th and 99th). In the case of a 2-mm cube, the induced electric field is averaged over 64 voxels. The global difference is the normalized average of point-wise absolute difference of the internal electric field distributions between SPFD and FEM computations (E_{SPFD} and E_{FEM} , respectively), as follows:

$$\text{Diff} [\%] = \frac{100}{\max_{n \in \Omega} (E_{\text{SPFD}}(n), E_{\text{FEM}}(n))} \times \frac{\sum_{n=1}^N |E_{\text{SPFD}}(n) - E_{\text{FEM}}(n)|}{N}. \quad (3)$$

III. NUMERICAL RESULTS

A. Internal Electric Field on The Brain

Figs. 2A-B show computed internal electric field strength on the brain cortex during TMS exposure over the vertex. Similar electric field distributions were obtained by two groups, i.e., by the two different electromagnetic solvers: SPFD and FEM. The difference of the voxel maximum value of the internal electric field is affected by the stair-casing error, as shown in Table I. The internal field maximum value shows less variation adopting the 99.9th and 99th percentiles with the maximum value substantially reduced by 60% using the 99th value.

The distributions of the electric fields in the whole brain (grey and white matter) show a good agreement (Fig. 2C) between the two different electromagnetic solvers. This is quantified by the global difference in Table I that shows a difference smaller than 3% considering the whole brain or target region.

In the following section III.B, the 99th percentile value of electric fields computed by the SPFD method is used to obtain the nerve activation for proper discussion of nerve modeling effect.

B. Nerve Modelling Verification

Verification of the stimulation threshold is conducted for

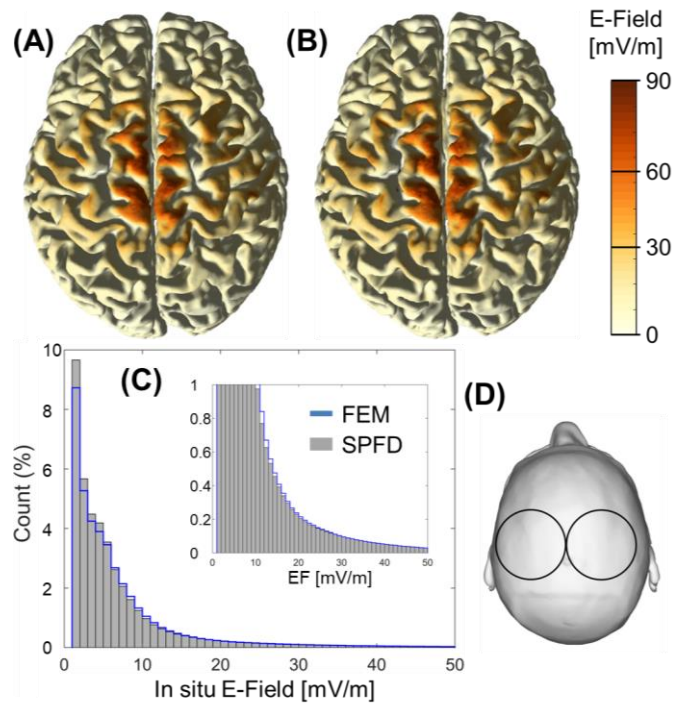


Fig. 2. Verification of the internal electric field on the brain cortex using (A) SPFD and (B) FEM numerical methods with input current of 1 A. (C) Distribution of the electric field in the whole brain (grey and white matter) with bins of 1 mV/m. (D) TMS coil location on the vertex position of the scalp.

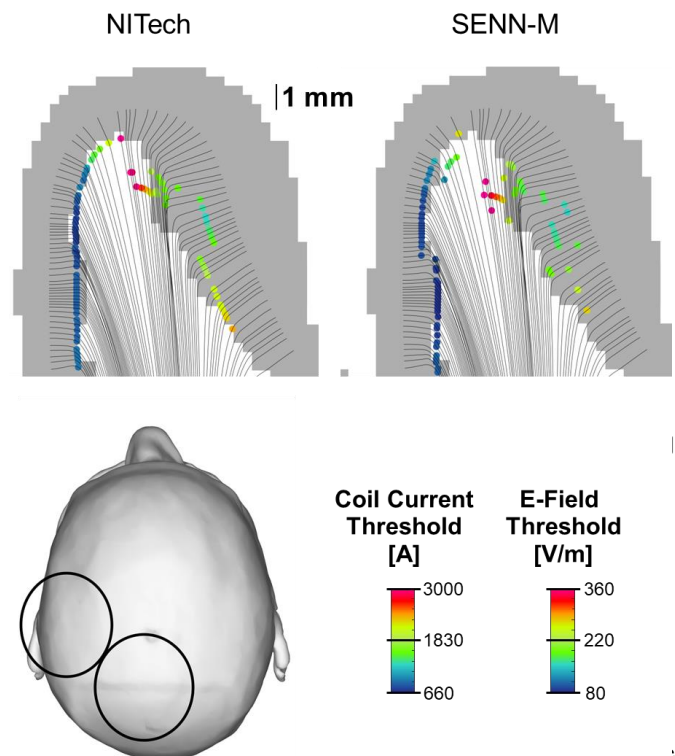


Fig. 3. Activation threshold intensity and location along the fibers axons ($10 \mu\text{m}$ of thickness) for NITech and SENN-M (independent implementation) for TMS targeting motor area as used in clinical practice.

TABLE I

COMPARISON OF ELECTRIC FIELD COMPUTED BY TWO ELECTROMAGNETIC METHODS.

Voxel Maximum Local Difference [%]			Global Difference [%]			
100% ile	99.9% ile	99 % ile	2-mm Cube 99.9%ile	2-mm Cube 99 % ile	Whole Brain	Target
189.2	0.73	0.41	3.32	1.77	0.15	2.7

TABLE II

VERIFICATION OF AXON ACTIVATION BY SENN AND NITECH NERVE AXON IMPLEMENTATION ($N = 90$ AXONS)

Metric	Value	Parameter (Table A.)	Parameter Variation		
			D (15 μ m)	g_s (0 mS/cm ²)	T (18°C)
Threshold	Mean	7.7	17.1	7.5	7.6
Relative Error [%]	Std	7.9	15.4	7.5	7.8
	Max	24.7	43.3	24.2	24.6
	Min	0.2	0.1	0.2	0.1
Position Difference [mm]	Mean	0.6	0.9	0.6	0.5
	Std	0.6	0.5	0.6	0.6
	Max	2.1	3.8	2.1	2.1
	Min	0.0	0.5	0.0	0.0

independent implementations of pyramidal axon models embedded in the motor hand area (Fig. 1A). The stimulation thresholds correspond to the internal electric field strength or the external magnetic field, as shown in Fig. 3. Good agreement is observed between the NITech and SENN-M implementations. The mean relative difference of the stimulation thresholds is 7.7% (0.2-24.7%) between NITech and SENN-M. The larger differences are observed at the distal gyral bank (right side). The distance error of the stimulation position is 0.6 ± 0.6 mm, which is close to the model resolution. The effects of variation of temperature and myelination did not affect the results, although higher fiber diameter may produce more variation of the results, as shown in Table II.

C. Permissible Field Strength

Threshold-frequency curves were derived from uniform exposure of the axon nerves (NITech model) and compared with permissible exposure levels prescribed in ICNIRP and IEEE. Fig. 4 shows that permissible external magnetic field strength and internal electric field in the current guidelines/standards, which are conservative with different factors over the frequency range. Specifically, the IEEE reference level is smaller with factors of 10–150 and 20–80 for the internal electric field and external magnetic field, respectively in a controlled environment. ICNIRP occupational basic restriction and reference level are smaller by a factor of 30–165 and 140–650, respectively. The higher and lower factors are for 1 kHz and 100 kHz to 10 MHz, respectively.

D. Potential Stimulation for Non-Uniform Field Exposure from WPT System.

We investigated the possible activation of cortical axons by WPT system for three different head positions (Fig. 1C). For commercial transmitting power of 3.7 kW, we did not find activation of any axons of the hand motor area, and the internal electric field values were considerably higher than basic restriction in general public for CNS/brain tissues at 85 kHz

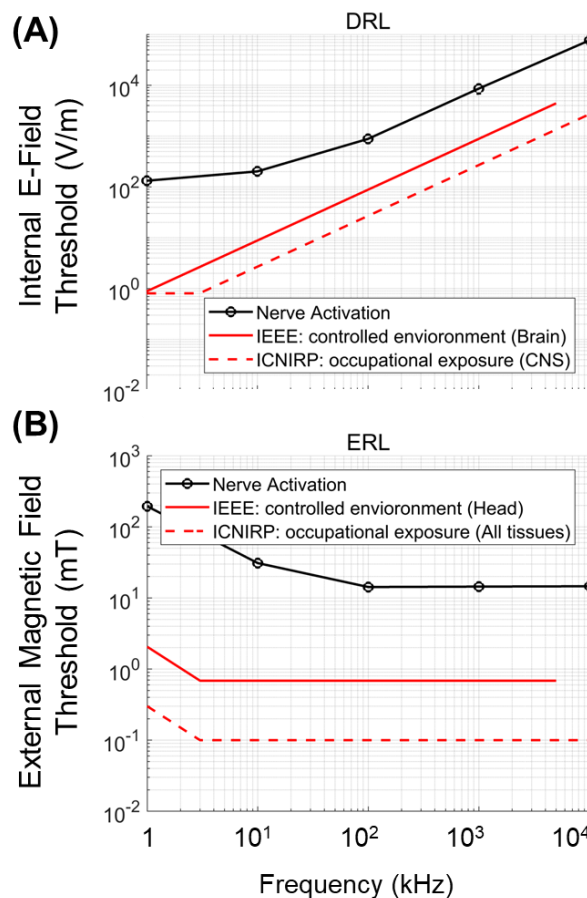


Fig. 4. Excitation thresholds for uniform exposure compared with ICNIRP guidelines and IEEE safety standard. (A) Dosimetry reference level. (B) Exposure reference level. Minimum threshold was selected between nerves in Fig. 1A for each frequency.

TABLE III
WPT EXPOSURE DOSIMETRY ANALYSIS IN THE BRAIN
($P_0 = 3.7$ kW OF TRANSMITTING POWER)

Head Position ^a	Cortical Axon Activation	Multiplier factor of P_0	Internal E-Field [V/m]		
			100% ile	99.9 % ile	99% ile
I	No	1	0.131	0.081	0.063
II	Activation	1	0.265	0.146	0.109
III	Activation	1	0.115	0.058	0.040
I		10,250	17.5	8.6	6.1
II	Activation	43,320	55.2	30.4	22.7
III		28,630	36.0	15.8	11.3

^aHead positions as shown in Fig. 1C

(25.03 V/m and 11.47 V/m for IEEE standard and ICNIRP guidelines, respectively). For axonal activation, the transmitting power should be more than 10,000 times, as shown in Table III.

IV. DISCUSSION AND CONCLUSIONS

This study investigated cortical stimulation threshold by combined modelling of electromagnetic dosimetry and neuron models for exposure at intermediate frequencies. The computed internal electric field is corroborated by two different methods (SPFD and FEM), and verification of pyramidal axons modelling results was conducted for medical application of TMS, in which the excitation threshold can be obtained for the measurable physiological marker (MEP). The results were

compared with the permissible levels defined by the guidelines/standards.

The voxel maximum of an internal electric field is affected by the staircase error (inherent when using voxelized anatomical models) [59]. Analytical solutions for multi-spherical models of the head tissues have shown that suppression of numerical artifacts by using the 99.9th percentile method is effective for grey matter tissue for magnetic exposure [60]. However, the computation of induced electric field is challenging because no analytical solutions exist for anatomical head models. **Intercomparison becomes important for assessing stability of the computation. It has been conducted for uniform exposure at intermedia frequencies [56], [61]–[63].** Also, a preliminary inter-comparison has been conducted in TMS [64], which did not consider the activation for a specific target (like motor area in this study). As indirect verification, our results confirmed that 99.9th and 99th percentiles are stable for two different numerical methods (SPFD and FEM), as shown in Table I. Moreover, the verification of the electric field should consider not only its maximum value but also its distribution as the nerve activation can also occur at a point with a high field-gradient along the axon pathway (i.e., bends) [65], unlike [64]. The comparison of the distribution between the two groups showed a good agreement in Fig. 2 and Table I.

TMS-induced electric field activation of axons of the corticospinal tracts showed in situ electric fields (99.9th percentile) between 80 V/m and 200 V/m that agrees with reported intensities for generating a motor response [66], [67]. In addition, the activation thresholds were confirmed by two independent implementations of the CRRSS model (7.7% of the relative difference in a group of axons), the stimulation site occurred consistently at the bend due to a higher electric field gradient (mean distance error of 0.6 mm). Except for the fiber diameter, other nerve parameters did not affect the agreement between the two implementations. As a larger diameter decreases the number of nodes in the axon, its relative positions to maximum bending may affect the results during the discretization process. This will be addressed in future work.

To frequencies above 400 Hz and 750 Hz, the ICNIRP basic restrictions and IEEE dosimetry reference are based on peripheral nerve system (PNS), respectively. Consequently, this study investigated permissible levels at frequencies higher than 1 kHz (not synaptic effect) but using CNS direct axonal stimulation considering the importance of brain tissues during electromagnetic head exposure. One of the reasons for this is that PNS activation is not necessarily an adverse health effect, such as the sensation of skin responses. To derive the threshold level for the CNS would be helpful for the scientific rationale of the guidelines/standard. Based on the verified multi-scale modelling (electromagnetic dosimetry combined with axon models), the derived permissible level in Fig. 4 for uniform exposure showed that allowable external magnetic field strength and internal electric field established in both guidelines/standards are significantly lower than the internal electric field needed for the stimulation of the central nervous system for medical applications [28] in particular for the range of below 100 kHz. The conservativeness from the guidelines/standards was expected [28], considering that the stimulation threshold of PNS is smaller than CNS direct axonal activation for frequencies larger than 1kHz. For lower

frequencies, the ICNIRP guideline and IEEE standard use phosphenes and synapse effects but these are not considered in this study. Synaptic effects are expected to occur at lower thresholds than direct axonal activation, but the rationality is not clear, and synapse and axonal depolarization/activation should be considered in future studies.

This multiscale modelling approach was also applied to investigate the effects of neuronal activation for a high-power charge of electric vehicles. The maximum transmitting power for charging vehicles is expected to be several kilowatts (7 kW [68]–[70]). We did not observe axonal activation for this transmitting power, and ten times higher power was required to obtain axonal activation in the motor cortex for WPT. Also, body posture and size, which are not considered systematically, would be an additional variability to be considered [54].

In conclusion, this is the first intercomparison for multiscale simulation approach that was applied to derive permissible external field strength for central nervous tissues at intermediate frequencies. We also presented the first application of multi-scale modelling for compliance analysis of WPT. Internal electric fields established in both guidelines are significantly lower than the internal electric field needed for CNS stimulation for medical applications for the range of below 100 kHz. In the future, more subjects and different axonal models need to be considered to derive the reference levels due to high inter-subject variability.

APPENDIX

TABLE A
NERVE MODEL PARAMETERS AND IMPLEMENTATION

Parameter	Sym	Value	Units
Outer diameter	D	10	[μm]
Inner diameter	d	0.64D	
Internodal length	L	100D	
Ranvier node length	l_n	1.5×10^{-4}	[cm]
No. of myelin layers	N_m	$75 \times 10^4 D$	
Axoplasmatic resistivity	ρ_a	0.07	[$\text{k}\Omega \cdot \text{cm}$]
Extracellular resistivity	ρ_e	0.3	[$\text{k}\Omega \cdot \text{cm}$]
Myelin conductance/layer	g_i	1	[mS/cm^2]
Membrane capacitance	c_m	1	[$\mu\text{F}/\text{cm}^2$]
Sodium conductance	g_{Na}	1445	[mS/cm^2]
Leak conductance	g_l	128	[mS/cm^2]
Sodium Nernst potential	E_{Na}	115	[mV]
Leak Nernst potential	E_l	-0.01	[mV]
Probability for opening the ionic channels	m_0	0.003	
	h_0	0.75	
Temperature	T	37	[$^{\circ}\text{C}$]
Implementation		NITech	SENN-M
Segments/section	1		1
Boundary conditions	Clamped		Clamped
Discretization Time step	Absolute/relative tolerances		$\min(25 \mu\text{s}, T_p/75)$
	1 μs and 1 ms		
Solver	ode15s variable-step, variable-order (VSVO)		Staggered Crank-Nicholson
Total Length		1.5 – 2.5 [cm]	

REFERENCES

- [1] IEEE, *IEEE standard for safety levels with respect to human exposure to electromagnetic fields, 0-3kHz*. Institute of Electrical and Electronics Engineers, 2002.
- [2] ICNIRP, "Guidelines for limiting exposure to time-varying electric, magnetic, and electromagnetic fields (up to 300 GHz). International Commission on Non-Ionizing Radiation Protection," *Health Phys.*, vol. 74, no. 4, pp. 494–522, Apr. 1998.
- [3] World Health Organization, "Electromagnetic fields and public health Intermediate Frequencies (IF)," *Int. EMF Proj. Inf. Sheet*, pp. 1–4, 2005.
- [4] S. Aerts, C. Calderon, B. Valič, M. Maslanyj, D. Addison, T. Mee, C. Goiceanu, L. Verloock, M. Van den Bossche, P. Gajšek, R. Vermeulen, M. Rössli, E. Cardis, L. Martens, and W. Joseph, "Measurements of intermediate-frequency electric and magnetic fields in households," *Environ. Res.*, vol. 154, pp. 160–170, Apr. 2017.
- [5] ICNIRP, "Guidelines for limiting exposure to time-varying electric and magnetic fields (1 Hz to 100 kHz)," *Health Phys.*, vol. 99, no. 6, pp. 818–36, Dec. 2010.
- [6] J. P. Reilly and A. Hirata, "Low-frequency electrical dosimetry: research agenda of the IEEE International Committee on Electromagnetic Safety," *Phys. Med. Biol.*, vol. 61, no. 12, pp. R138–R149, Jun. 2016.
- [7] K. Wake, I. Laakso, A. Hirata, J. Chakarothai, T. Onishi, S. Watanabe, V. De Santis, M. Feliziani, and M. Taki, "Derivation of Coupling Factors for Different Wireless Power Transfer Systems: Inter- and Intralaboratory Comparison," *IEEE Trans. Electromagn. Compat.*, vol. 59, no. 2, pp. 677–685, Apr. 2017.
- [8] X. L. Chen, A. E. Umenei, D. W. Baarman, N. Chavannes, V. De Santis, J. R. Mosig, and N. Kuster, "Human Exposure to Close-Range Resonant Wireless Power Transfer Systems as a Function of Design Parameters," *IEEE Trans. Electromagn. Compat.*, vol. 56, no. 5, pp. 1027–1034, Oct. 2014.
- [9] I. Laakso, S. Tsuchida, A. Hirata, and Y. Kamimura, "Evaluation of SAR in a human body model due to wireless power transmission in the 10 MHz band," *Phys. Med. Biol.*, vol. 57, no. 15, pp. 4991–5002, Aug. 2012.
- [10] M. Koohestani, M. Zhadobov, and M. Ettore, "Design Methodology of a Printed WPT System for HF-Band Mid-Range Applications Considering Human Safety Regulations," *IEEE Trans. Microw. Theory Tech.*, vol. 65, no. 1, pp. 270–279, Jan. 2017.
- [11] Y. Aoki, T. Arima, T. Uno, J. Chakarothai, K. Wake, K. Fujii, and S. Watanabe, "Calculation of coupling factor for kHz-band wireless power transfer system using numerical human models," in *2015 International Workshop on Electromagnetics: Applications and Student Innovation Competition (IWEM)*, 2015, pp. 1–2.
- [12] T. Hikage, T. Nojima, and H. Fujimoto, "Active implantable medical device EMI assessment for wireless power transfer operating in LF and HF bands," *Phys. Med. Biol.*, vol. 61, no. 12, pp. 4522–4536, Jun. 2016.
- [13] F. Wen, X. Huang, F. Wen, and X. Huang, "Human Exposure to Electromagnetic Fields from Parallel Wireless Power Transfer Systems," *Int. J. Environ. Res. Public Health*, vol. 14, no. 2, p. 157, Feb. 2017.
- [14] M. Koohestani, M. Ettore, and M. Zhadobov, "Local Dosimetry Applied to Wireless Power Transfer Around 10 MHz: Dependence on EM Parameters and Tissues Morphology," *IEEE J. Electromagn. RF Microwaves Med. Biol.*, vol. 2, no. 2, pp. 123–130, Jun. 2018.
- [15] C. Cimala, M. Clemens, J. Streckert, and B. Schmuelling, "High-resolution magnetic-field exposure simulations of automotive inductive power-transfer systems using a scaled-frequency finite difference time domain approach with multi-GPU acceleration," *Int. J. Numer. Model. Electron. Networks, Devices Fields*, vol. 31, no. 2, p. e2231, Mar. 2018.
- [16] J. Chakarothai, K. Wake, T. Arima, S. Watanabe, and T. Uno, "Exposure Evaluation of an Actual Wireless Power Transfer System for an Electric Vehicle With Near-Field Measurement," *IEEE Trans. Microw. Theory Tech.*, vol. 66, no. 3, pp. 1543–1552, Mar. 2018.
- [17] V. De Santis, T. Campi, S. Cruciani, I. Laakso, and M. Feliziani, "Assessment of the Induced Electric Fields in a Carbon-Fiber Electrical Vehicle Equipped with a Wireless Power Transfer System," *Energies*, vol. 11, no. 3, p. 684, Mar. 2018.
- [18] I. Laakso and A. Hirata, "Evaluation of the induced electric field and compliance procedure for a wireless power transfer system in an electrical vehicle," *Phys. Med. Biol.*, vol. 58, no. 21, pp. 7583–7593, Nov. 2013.
- [19] I. A. Shah and H. Yoo, "Assessing Human Exposure With Medical Implants to Electromagnetic Fields From a Wireless Power Transmission System in an Electric Vehicle," *IEEE Trans. Electromagn. Compat.*, pp. 1–8, 2019.
- [20] J. Lin, M. Lu, T. Wu, L. Yang, and T. Wu, "Evaluating extremely low frequency magnetic fields in the rear seats of the electric vehicles," *Radiat. Prot. Dosimetry*, vol. 182, no. 2, pp. 190–199, Dec. 2018.
- [21] Y. Suzuki and M. Taki, "Measurement of magnetic field from an induction heating hob and estimation of induced current density in human body," *IEEJ Trans. Fundam. Mater.*, vol. 125, no. 5, pp. 427–433, 2005.
- [22] B. Kos, B. Valič, D. Miklavčič, T. Kotnik, and P. Gajšek, "Pre- and post-natal exposure of children to EMF generated by domestic induction cookers," *Phys. Med. Biol.*, vol. 56, no. 19, pp. 6149–6160, Oct. 2011.
- [23] A. Christ, R. Guldemann, B. Bühlmann, M. Zefferer, J. F. Bakker, G. C. van Rhoon, and N. Kuster, "Exposure of the Human Body to Professional and Domestic Induction Cooktops Compared to the Basic Restrictions," *Bioelectromagnetics*, vol. 33, no. 8, pp. 695–705, Dec. 2012.
- [24] R. Leo and T. Latif, "Repetitive Transcranial Magnetic Stimulation (rTMS) in Experimentally Induced and Chronic Neuropathic Pain: A Review," *J. Pain*, vol. 8, no. 6, pp. 453–459, Jun. 2007.
- [25] H. Seo, N. Schaworonkow, S. C. Jun, and J. Triesch, "A multi-scale computational model of the effects of TMS on motor cortex," *FL000Research*, vol. 5, p. 1945, May 2017.
- [26] A. Nummenmaa, M. Stenroos, R. J. Ilmoniemi, Y. C. Okada, M. S. Hämäläinen, and T. Raij, "Comparison of spherical and realistically shaped boundary element head models for transcranial magnetic stimulation navigation," *Clin. Neurophysiol.*, vol. 124, no. 10, pp. 1995–2007, Oct. 2013.
- [27] B. D. Goodwin and C. R. Butson, "Subject-Specific Multiscale Modeling to Investigate Effects of Transcranial Magnetic Stimulation," *Neuromodulation Technol. Neural Interface*, vol. 18, no. 8, pp. 694–704, Dec. 2015.
- [28] M. Soldati, M. Mikkonen, I. Laakso, T. Murakami, Y. Ugawa, and A. Hirata, "A multi-scale computational approach based on TMS experiments for the assessment of electro-stimulation thresholds of the brain at intermediate frequencies," *Phys. Med. Biol.*, vol. 63, no. 22, p. 225006, Nov. 2018.
- [29] J. Gomez-Tames, H. Akimasa, M. Tamura, and Y. Muragaki, "Corticomotoneuronal Model for Intraoperative Neurophysiological Monitoring During Direct Brain Stimulation," *Int. J. Neural Syst.*, Jun. 2018.
- [30] A. M. Samoudi, S. Kampusch, E. Tanghe, J. C. Széles, L. Martens, E. Kaniasas, and W. Joseph, "Numerical modeling of percutaneous auricular vagus nerve stimulation: a realistic 3D model to evaluate sensitivity of neural activation to electrode position," *Med. Biol. Eng. Comput.*, vol. 55, no. 10, pp. 1763–1772, Oct. 2017.
- [31] E. Neufeld, A. M. Cassará, H. Montanaro, N. Kuster, and W. Kainz, "Functionalized anatomical models for EM-neuron Interaction modeling," *Phys. Med. Biol.*, vol. 61, no. 12, pp. 4390–4401, Jun. 2016.
- [32] A. Hirata, I. Laakso, J. Gomez-Tames, and H. Hontani, "Combined simulation of bioelectromagnetics and nerve activation and its application," *IEEJ Trans. Fundam. Mater.*, vol. 138, no. 6, pp. 265–270, Jun. 2018.
- [33] J. Gomez-Tames, T. Kutsuna, M. Tamura, Y. Muragaki, and A. Hirata, "Intraoperative direct subcortical stimulation: comparison of monopolar and bipolar stimulation," *Phys. Med. Biol.*, vol. 63, no. 22, p. 225013, Nov. 2018.
- [34] A. T. Barker, R. Jalinous, and I. L. Freeston, "Non-invasive magnetic stimulation of human motor cortex," *Lancet (London, England)*, vol. 1, no. 8437, pp. 1106–7, May 1985.
- [35] S. Ueno, T. Tashiro, and K. Harada, "Localized stimulation of neural tissues in the brain by means of a paired configuration of time-varying magnetic fields," *J. Appl. Phys.*, vol. 64, no. 10, pp. 5862–5864, Nov. 1988.
- [36] J. Gomez-Tames, T. Tarnaud, T. Van De Seenem, E. Rashed, A.

- Hirata, L. Martens, E. Tanghe, and W. Joseph, "Setting Reference Level in Human Safety Guidelines via Cortical Nerve Activation Intercomparison at IF," in *International Symposium on Electromagnetic Compatibility*, 2019.
- [37] J. Gomez-Tames, A. Hamasaka, I. Laakso, A. Hirata, and Y. Ugawa, "Atlas of optimal coil orientation and position for TMS: A computational study," *Brain Stimul.*, vol. 11, no. 4, pp. 839–848, Apr. 2018.
- [38] M. Iwahashi, J. Gomez-Tames, I. Laakso, and A. Hirata, "Evaluation method for *in situ* electric field in standardized human brain for different transcranial magnetic stimulation coils," *Phys. Med. Biol.*, vol. 62, no. 6, pp. 2224–2238, Mar. 2017.
- [39] T. Dawson and M. Stuchly, "Analytic validation of a three-dimensional scalar-potential finite-difference code for low-frequency magnetic induction," *Appl. Comput. Electromagn. Soc. J.*, vol. 11, pp. 72–81, 1996.
- [40] A. Hirata, F. Ito, and I. Laakso, "Confirmation of quasi-static approximation in SAR evaluation for a wireless power transfer system," *Phys. Med. Biol.*, vol. 58, no. 17, pp. N241–N249, Sep. 2013.
- [41] E. Neufeld, D. Szczerba, N. Chavannes, and N. Kuster, "A novel medical image data-based multi-physics simulation platform for computational life sciences," *Interface Focus*, vol. 3, no. 2, p. 20120058, Apr. 2013.
- [42] J. O. Nieminen, L. M. Koponen, and R. J. Ilmoniemi, "Experimental Characterization of the Electric Field Distribution Induced by TMS Devices," *Brain Stimul.*, vol. 8, no. 3, pp. 582–589, 2015.
- [43] S. Gabriel, R. W. Lau, and C. Gabriel, "The dielectric properties of biological tissues: III. Parametric models for the dielectric spectrum of tissues," *Phys. Med. Biol.*, vol. 41, no. 11, p. 2271, Nov. 1996.
- [44] K. Wake, K. Sasaki, and S. Watanabe, "Conductivities of epidermis, dermis, and subcutaneous tissue at intermediate frequencies," *Phys. Med. Biol.*, vol. 61, no. 12, pp. 4376–4389, Jun. 2016.
- [45] I. Laakso and A. Hirata, "Fast multigrid-based computation of the induced electric field for transcranial magnetic stimulation," *Phys. Med. Biol.*, vol. 57, no. 23, pp. 7753–7765, 2012.
- [46] J. P. Reilly, V. T. Freeman, and W. D. Larkin, "Sensory effects of transient electrical stimulation-evaluation with a neuroelectric model," *IEEE Trans. Biomed. Eng.*, vol. 32, no. 12, pp. 1001–11, Dec. 1985.
- [47] J. D. Sweeney, J. T. Mortimer, and D. Durand, "Modeling of mammalian myelinated nerve for functional neuromuscular electrostimulation," *IEEE 97th Annu. Conf. Eng. Med. Biol. Soc. Bost.*, vol. 9, pp. 1577–1578, 1987.
- [48] J. Gomez-Tames, Y. Fukuhara, S. He, K. Saito, K. Ito, and W. Yu, "A human-phantom coupling experiment and a dispersive simulation model for investigating the variation of dielectric properties of biological tissues," *Comput. Biol. Med.*, vol. 61, pp. 144–149, 2015.
- [49] T. Tarnaud, W. Joseph, L. Martens, and E. Tanghe, "Dependence of excitability indices on membrane channel dynamics, myelin impedance, electrode location and stimulus waveforms in myelinated and unmyelinated fibre models," *Med. Biol. Eng. Comput.*, vol. 56, no. 9, pp. 1595–1613, Sep. 2018.
- [50] L. Firmin, P. Field, M. A. Maier, A. Kraskov, P. A. Kirkwood, K. Nakajima, R. N. Lemon, and M. Glickstein, "Axon diameters and conduction velocities in the macaque pyramidal tract," *J. Neurophysiol.*, vol. 112, no. 6, pp. 1229–1240, 2014.
- [51] F. S. Salinas, J. L. Lancaster, and P. T. Fox, "Detailed 3D models of the induced electric field of transcranial magnetic stimulation coils," *Phys. Med. Biol.*, vol. 52, no. 10, pp. 2879–2892, May 2007.
- [52] P. I. Petrov, S. Mandija, I. E. C. Sommer, C. A. T. van den Berg, and S. F. W. Neggers, "How much detail is needed in modeling a transcranial magnetic stimulation figure-8 coil: Measurements and brain simulations," *PLoS One*, vol. 12, no. 6, p. e0178952, Jun. 2017.
- [53] T. Shimamoto, I. Laakso, and A. Hirata, "*In-situ* electric field in human body model in different postures for wireless power transfer system in an electrical vehicle," *Phys. Med. Biol.*, vol. 60, no. 1, pp. 163–173, Jan. 2015.
- [54] I. Laakso, A. Hirata, and O. Fujiwara, "Computational dosimetry for wireless charging of an electrical vehicle," *2014 Int. Symp. Electromagn. Compat.*, pp. 202–205, 2014.
- [55] J. Schneider, "Wireless Power Transfer for Light-Duty Plug-In/Electric Vehicles and Alignment Methodology - SAE International," 2016.
- [56] A. Hirata, K. Yamazaki, S. Hamada, Y. Kamimura, H. Taro, K. Wake, Y. Suzuki, N. Hayashi, and O. Fujiwara, "Intercomparison of induced fields in Japanese male model for ELF magnetic field exposures: effect of different computational methods and codes," *Radiat. Prot. Dosimetry*, vol. 138, no. 3, pp. 237–244, Mar. 2010.
- [57] T. Dawson, M. Potter, and M. Stuchly, "Evaluation of modeling accuracy of power frequency field interactions with the human body," *Appl. Comput. Electromagn. Soc. J.*, vol. 16, pp. 162–172, 2001.
- [58] Y. Diao, K. H. Chan, S. W. Leung, W. Sun, and Y. M. Siu, "Prediction of magnetic field emissions by current source reconstruction using radial basis function network," *Electron. Lett.*, vol. 51, no. 16, pp. 1243–1245, Aug. 2015.
- [59] I. Laakso and A. Hirata, "Reducing the staircasing error in computational dosimetry of low-frequency electromagnetic fields," *Phys. Med. Biol.*, vol. 57, no. 4, pp. N25–N34, Feb. 2012.
- [60] J. Gomez-Tames, I. Laakso, Y. Habu, A. Hirata, D. Poljak, and K. Yamazaki, "Computational Artifacts of the In Situ Electric Field in Anatomical Models Exposed to Low-Frequency Magnetic Field," *IEEE Trans. Electromagn. Compat.*, vol. 60, no. 3, pp. 589–597, 2017.
- [61] A. Hirata, Y. Takano, Y. Kamimura, and O. Fujiwara, "Effect of the averaging volume and algorithm on the *in situ* electric field for uniform electric- and magnetic-field exposures," *Phys. Med. Biol.*, vol. 55, no. 9, pp. N243–N252, May 2010.
- [62] K. Taguchi, I. Laakso, K. Aga, A. Hirata, Y. Diao, J. Chakarothai, and T. Kashiwa, "Relationship of external field strength with local and whole-body averaged specific absorption rates in anatomical human models," *IEEE Access*, vol. 6, pp. 70186–70196, 2018.
- [63] K. Aga, A. Hirata, and I. Laakso, "Relationship between In-Situ Electric Field and External Magnetic Field Strength in Human Models-Rational of IEEE C95.6 Standard Revisited," in *IEEE International Symposium on Electromagnetic Compatibility*, 2018, vol. 2018–August, pp. 515–520.
- [64] D. Poljak, M. Cvetkovic, O. Bottauscio, A. Hirata, I. Laakso, E. Neufeld, S. Reboux, C. Warren, A. Giannopoulos, and F. Costen, "On the Use of Conformal Models and Methods in Dosimetry for Nonuniform Field Exposure," *IEEE Trans. Electromagn. Compat.*, vol. 60, no. 2, pp. 328–337, Apr. 2018.
- [65] P. J. Maccabee, V. E. Amassian, L. P. Eberle, and R. Q. Cracco, "Magnetic coil stimulation of straight and bent amphibian and mammalian peripheral nerve in vitro: locus of excitation," *J. Physiol.*, vol. 460, pp. 201–19, Jan. 1993.
- [66] L. G. Cohen, B. J. Roth, J. Nilsson, N. Dang, M. Panizza, S. Bandinelli, W. Friauf, and M. Hallett, "Effects of coil design on delivery of focal magnetic stimulation. Technical considerations," *Electroencephalogr. Clin. Neurophysiol.*, vol. 75, no. 4, pp. 350–357, Apr. 1990.
- [67] I. Laakso, T. Murakami, A. Hirata, and Y. Ugawa, "Where and what TMS activates: Experiments and modeling," *Brain Stimul.*, Sep. 2017.
- [68] J. Deng, Fei Lu, S. Li, T.-D. Nguyen, and C. Mi, "Development of a high efficiency primary side controlled 7kW wireless power charger," in *2014 IEEE International Electric Vehicle Conference (IEVC)*, 2014, pp. 1–6.
- [69] M. Abou Houran, X. Yang, W. Chen, M. Abou Houran, X. Yang, and W. Chen, "Magnetically Coupled Resonance WPT: Review of Compensation Topologies, Resonator Structures with Misalignment, and EMI Diagnostics," *Electronics*, vol. 7, no. 11, p. 296, Nov. 2018.
- [70] T. M. Fisher, K. B. Farley, Y. Gao, H. Bai, and Z. T. H. Tse, "Electric vehicle wireless charging technology: a state-of-the-art review of magnetic coupling systems," *Wirel. Power Transf.*, vol. 1, no. 2, pp. 87–96, Sep. 2014.